Geophysical Research Letters

RESEARCH LETTER
10.1029/2019GL082916

Ice-Free Radiative Convection Drives Spring Mixing in a Large Lake

D. J. Cannon[1], C. D. Troy[1], Q. Liao[2], and H. A. Bootsma[2]

[1]Lyles School of Civil Engineering, Purdue University, West Lafayette, IN, USA, [2]School of Freshwater Sciences, University of Wisconsin-Milwaukee, Milwaukee, WI, USA

Key Points:
- Radiative convection drives strong, deep mixing during the vernal turnover in a large, ice-free lake (Lake Michigan)
- Temperature profiles show a diurnal cycle of full water column mixing each day followed by surface-cooled restratification overnight
- Radiative convection is linked to a multiple-order enhancement in turbulence characteristics, including both dissipation and diffusivity

Correspondence to:
D. J. Cannon,
cannond@purdue.edu

Citation:
Cannon, D. J., Troy, C. D., Liao, Q., & Bootsma, H. A. (2019). Ice-free radiative convection drives spring mixing in a large lake. *Geophysical Research Letters*, 46, 6811–6820. https://doi.org/10.1029/2019GL082916

Received 5 APR 2019
Accepted 4 JUN 2019
Accepted article online 11 JUN 2019
Published online 28 JUN 2019

Abstract In this work we highlight the importance of radiative convection as a mixing mechanism in a large, ice-free lake (Lake Michigan, USA), where solar heating of waters below the temperature of maximum density drives vertical convection during the vernal turnover. Measurements taken over a 2-week period at a 55-m deep site demonstrate the ability of radiative convection to mix the entire water column. Observations show a diurnal cycle in which solar heating drives a steady deepening of the convective mixed layer throughout the day ($dH_{CML}/dt = 12.8$ m/hr), followed by surface-cooling-induced restratification during the night. Radiative convection is linked to a dramatic enhancement in turbulence characteristics, including both turbulent kinetic energy dissipation (ϵ: 10^{-9}–10^{-7} W/kg) and turbulent scalar diffusivity (K_z: 10^{-3}–10^{-1} m^2/s), suggesting that radiative convection plays a major role in driving vertical mixing throughout the water column during the *isothermal* spring.

Plain Language Summary When freshwater lakes fall below the temperature of maximum density ($T_{MD} \approx 4$ °C), solar-driven radiative convection can become a major source of turbulent mixing. As the sun heats near-surface waters, the denser (warmer) waters sink rapidly throughout the water column, driving increased mixing and vertical transport. In the current paper, we highlight the importance of this mixing mechanism as observed during a 2-week experiment at a 55-m deep site in a large, ice-free lake (Lake Michigan, USA). Observations demonstrate a daily cycle in which solar heating drives energetic, full water column mixing throughout the day, followed by significant surface cooling and restratification overnight. We show that radiative convection is linked to dramatic enhancements in turbulence characteristics. This suggests that convection plays a major role in setting spring mixing conditions throughout the Laurentian Great Lakes, with important implications for both biological and chemical species. This work represents one of the first observations of radiative convection in an ice-free lake, providing important insight for other large midlatitude lakes.

1. Introduction

For many inland lakes, where wind stress is relatively weak and tidal forcing is absent, convection plays an important role in shaping stratification and driving vertical transport (Bouffard & Wüest, 2019). This is especially true during the vernal turnover in dimictic lakes, when near-surface waters below the temperature of maximum density ($T_{MD} \approx 4$ °C) experience *radiative* convection; as daily radiative (solar) heating increases water temperatures throughout the photic zone, these heavier, gravitationally unstable surface waters sink, driving enhanced turbulent mixing. Recent work has established radiative convection as a dominant mixing mechanism in ice-covered lakes (Bouffard et al., 2019; Jonas, Terzhevik, et al., 2003; Yang et al., 2017), but its potential importance in nearly ice-free dimictic lakes has been largely speculative (e.g., Boyce et al., 1989). Large radiative heat fluxes in the Laurentian Great Lakes, attributed to high water clarity (Barbiero et al., 2018) and low ice cover (Wang et al., 2011), make them particularly susceptible to this phenomenon. Although ice-free radiative convection has been observed throughout the spring heating period (March–June; see Figure 1) in the Laurentian Great Lakes (Lake Michigan: Church, 1947; Beletsky & Schwab, 2001; Lake Superior: Bennett, 1978; Austin, 2019; and Lake Ontario: Scavia & Bennett, 1980), there have been, to the best of our knowledge, no direct observations of the turbulence characteristics associated with this mixing mechanism, despite its potential importance for both biological and chemical properties, including phytoplankton and zooplankton biomass (Sommer et al., 2012; Vanderploeg et al., 2010), dissolved oxygen (Yang et al., 2017), and nutrients (Hampton et al., 2017).

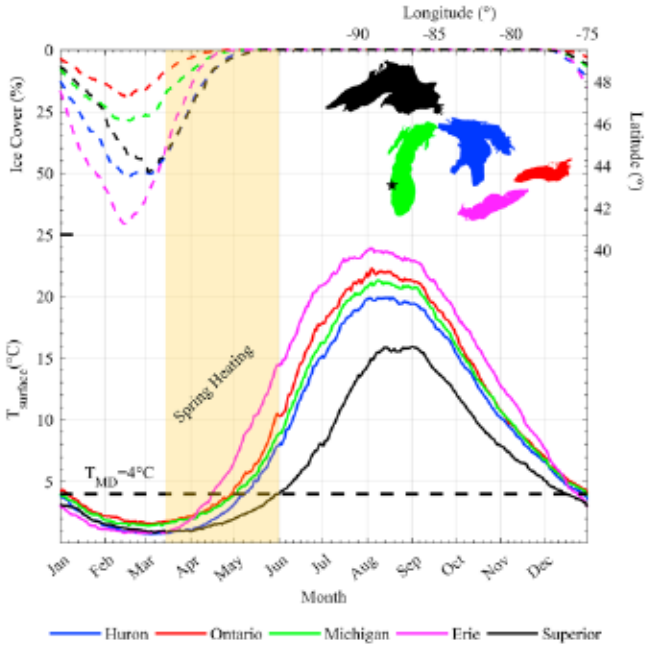

Figure 1. Average lake-wide surface temperature (°C; solid lines) and ice cover (%; dashed lines) as observed in the Laurentian Great Lakes between 1992 and 2017. The temperature of maximum density ($T_{MD} \approx 4$ °C) and the spring heating period are included for reference, as is an inset map of all five lakes (sample site: star). Source: NOAA Great Lakes CoastWatch (Leshkevich et al., 2018).

In this paper, we provide direct evidence of elevated mixing associated with ice-free radiative convection in large, deep lakes. Field measurements were collected during the ice-free spring turnover period in Lake Michigan (55-m depth) near Milwaukee, Wisconsin (USA) as part of a larger study examining the importance of turbulent mixing in regulating plankton and nutrient dynamics. To our knowledge, this research presents the first direct measurements of turbulent mixing associated with ice-free radiative convection in large lakes, providing conclusive evidence for the importance of this mechanism in driving vertical exchange.

2. Methods

2.1. Observations

A 15-day (5–20 April 2018) mooring deployment and microstructure campaign was used to obtain high-resolution measurements of mean flow, stratification, and turbulence in Lake Michigan at a 55-m deep site located near Milwaukee, Wisconsin, USA (43°04′27″N,87°45′14″W; Figure 1), a location for which we have previously reported both hydrodynamic (Cannon & Troy, 2018; Troy et al., 2016) and biogeochemical conditions (Mosley & Bootsma, 2015; Shen et al., 2018). An instrumented tripod equipped with two acoustic current profilers and a thermistor string was deployed throughout the experiment, while vertical profiles of velocity shear and temperature were collected during three separate profiling days (5, 12, and 20 April). The measurement period was selected such that the water column was nearly isothermal and surface temperatures were below the temperature of maximum density ($T_{surface} < 4$ °C).

Currents and mean shear were measured using two high-resolution acoustic velocimeters. Bottom boundary layer velocities (20–140 cm above bottom) were measured using a Nortek Aquadopp HR profiler, which was burst sampled at 2 Hz for 512 s every 10 min. A five-beam Nortek Signature 500 was used to measure mean currents continuously at a sample rate of 2 Hz outside of the bottom boundary layer (2.5–45 m above the bottom; 1-m bins). The raw data from all velocimeters were filtered according to manufacturer recommendations for signal-to-noise and correlation metrics.

Water column temperatures were measured using a combination of six SBE-56 (accuracy: ±0.002 °C; sample rate: 2 Hz) and 12 RBR TR-1060 (accuracy: ±0.002 °C; sample rate: 1 Hz) thermistors, which were deployed with 4-m spacing between 10- and 50-m depth, with more dense spacing (1 m) near the boundaries (5–7-m depth; 52–55-m depth). Potential water densities (ρ_θ) were calculated using the freshwater equation of state described by Tanaka et al. (2001), and potential density profiles were converted to local buoyancy frequencies (N^2) following Gill (1982) such that $N^2 = -\frac{g}{\rho_o}\frac{d\rho_\theta}{dz}$, where $g = 9.81$ m/s^2 is the gravitational constant and ρ_o is a reference density (taken as the mean density between points of interest). Temperature measurements were averaged over 60 s to reduce measurement uncertainty, resulting in an estimated buoyancy frequency threshold of $N^2 > 1.6 \times 10^{-7}$ rad^2/s^2.

External forcing conditions, including wind speed, cloud cover, relative humidity, air temperature, and water surface temperature, were obtained from the Great Lakes Coastal Forecasting System (http://glos.us/data-tools/point-query-tool-glcfs; Last Accessed: 15 October 2018). Wind stresses were estimated using wind-water drag coefficients and estimated wind speeds (Wüest & Lorke, 2003), while incoming shortwave solar radiation (E_o) was estimated using the equations presented in Martin et al. (1999). These shortwave radiation estimates were compared to both land-based weather stations and on-site measurements for verification. The vertical profile of penetrative solar radiation $E(z)$ was estimated using a two-layer exponential model:

$$E(z) = E_o\left[a_1 e^{-zk_1} + a_2 e^{-zk_2}\right] \quad (1)$$

where z is the depth below the water surface and E_o is defined as above. Light extinction coefficients (k_1=1.39, k_2=0.13 m^{-1}) and light absorption constants (a_1=0.36, a_2=0.47) were fit to vertical profiles

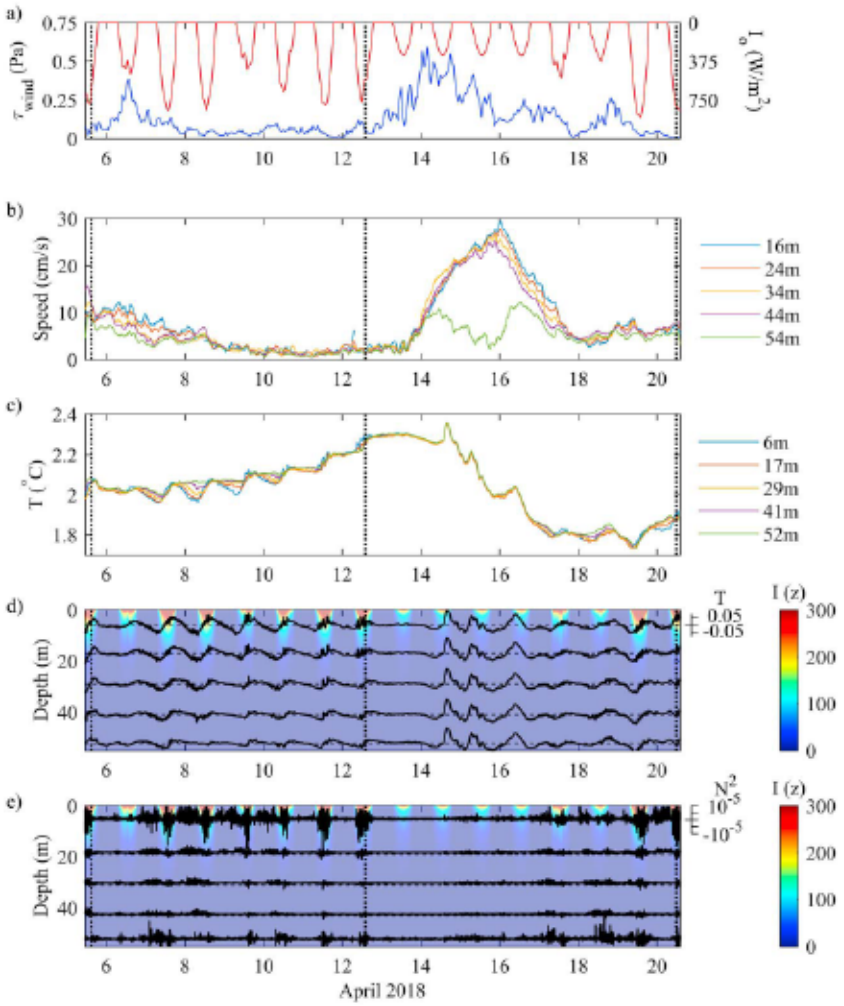

Figure 2. Water column overview including (a) wind stress (τ_{wind}; blue) and estimated incoming shortwave radiation (I_o; red), (b) current speed at various depths, (c) water column temperature at various depths, (d) 24-hr detrended temperature fluctuations (°C), and (e) buoyancy frequencies (N^2; rad^2/s^2). Microstructure measurement times are shown as vertical dashed lines, and subplots (e–d) are colored by shortwave radiation at depth ($I(z)$; W/m^2).

of $E(z)$ collected at the sample site during microstructure profiling campaigns. Solar radiation $E(z)$ estimates were converted to kinematic heat fluxes using the relation $I(z) = \frac{E(z)}{\rho c_p}$, where ρ is the in situ water density and $c_p = 4.2 \times 10^3$ J/kg K is the specific heat of water at constant pressure (Bouffard et al., 2016).

The buoyancy flux (B) was estimated using temperature measurements and the 1-D heat budget, such that

$$B(z) = \int_z^H g\alpha(z)\frac{\partial I}{\partial z}(z)dz + \int_z^H g\alpha(z)\frac{\partial T}{\partial t}(z)dz \tag{2}$$

where H is the water depth (55 m), $\alpha = -\rho^{-1}\partial\rho/\partial T$ is the thermal expansion coefficient, and $\frac{\partial T}{\partial t}(z)$ is the time rate of change of temperature (Jonas, Terzhevik, et al., 2003). In the current study, the buoyancy flux (B) is defined positive into the water column and it is assumed that observed temperature variations are driven entirely by solar radiation and vertical turbulent mixing. Temperature measurements were averaged and resampled at 1-hr intervals to reduce instrument uncertainties in gradient estimates. Turbulent scalar diffusivities (K_z) were calculated from the buoyancy flux such that

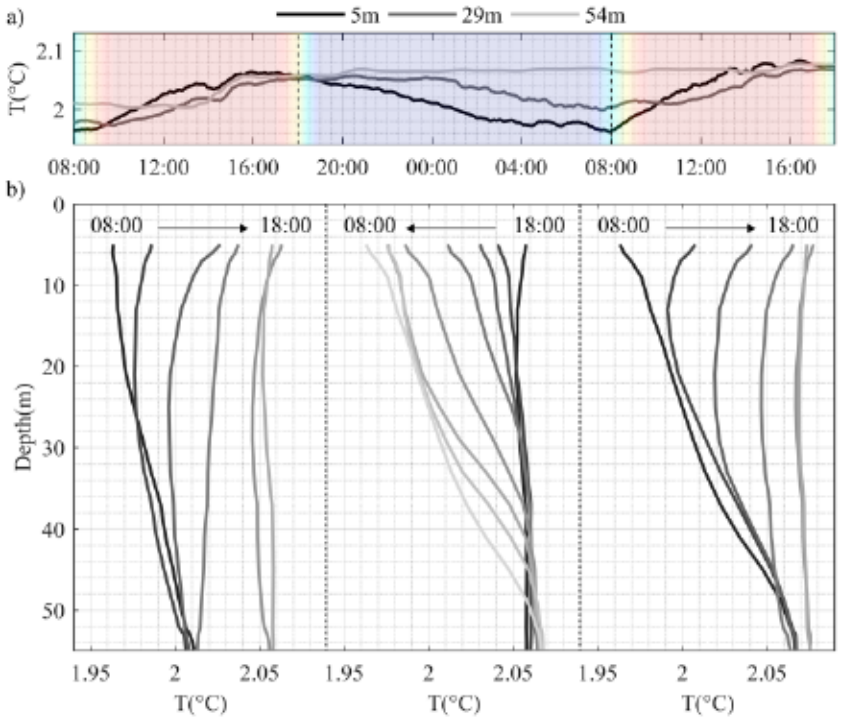

Figure 3. Representative 34-hr cycle of temperature profiles (1 hr smoothed), measured between 08:00 7 April and 18:00 8 April (local time), includes (a) time series of temperature measurements at 5-, 29-, and 54-m depth colored by estimated incoming shortwave radiation (warm colors: +; blue: zero) and (b) subsequent profiles of temperature over a single warming-cooling-warming cycle (2-hr increments).

$$K_z(z) = \frac{-B(z)}{g\alpha(z)[dT/dz(z)]} \tag{3}$$

where $\frac{\partial T}{\partial z}(z)$ is the vertical gradient of temperature and all other terms are defined as above. The 1-D heat budget estimates of buoyancy flux and turbulent diffusivity were restricted to periods of strong vertical convection and weak lateral advection; no diurnal cross-shelf transport patterns were observed, indicating that differential cooling was not affecting the measurement site.

2.2. Microstructure Data Analysis

For this study, 129 microstructure profiles were collected over three days (5, 12, and 20 April). Measurements were collected using a RSI MicroCTD (Rockland Scientific International, Inc.), which sampled shear and temperature microstructure at 512 Hz, free falling at a velocity of 0.8 m/s (vertical resolution: 1.5 mm). Microstructure measurements were limited to periods with weak wind forcing and moderate wave heights, which are favorable conditions for buoyancy-driven mixing. Shear microstructure was analyzed to obtain turbulent kinetic energy dissipation (ϵ), and temperature microstructure was used to quantify water column instability and overturning.

The energy spectra of vertical velocity shear were used to estimate turbulent kinetic energy dissipation (ϵ) using a combination of power spectral density function integration (Osborn, 1974) and Nasmyth empirical spectrum fitting (Bluteau et al., 2016). Energy spectra were calculated from 2 s (1,024 samples) measurement intervals overlapped by 50% (vertical resolution: 0.8 m), with corrections for both instrument accelerations (Goodman et al., 2006) and probe-induced spatial averaging (Macoun & Lueck, 2004). Dissipation algorithms were provided by the manufacturer (RSI) and additional details for this method can be found in Lueck (2013). Following Bluteau et al. (2016), the mean absolute deviation (MAD) was used to identify and discard all observed spectra that were affected by anisotropy or deviated significantly from the shape of the model spectrum, with a rejection criteria of MAD > $2(2/d)^{1/2}$, where d is degrees of freedom of the observed spectra (Ruddick et al., 2000).

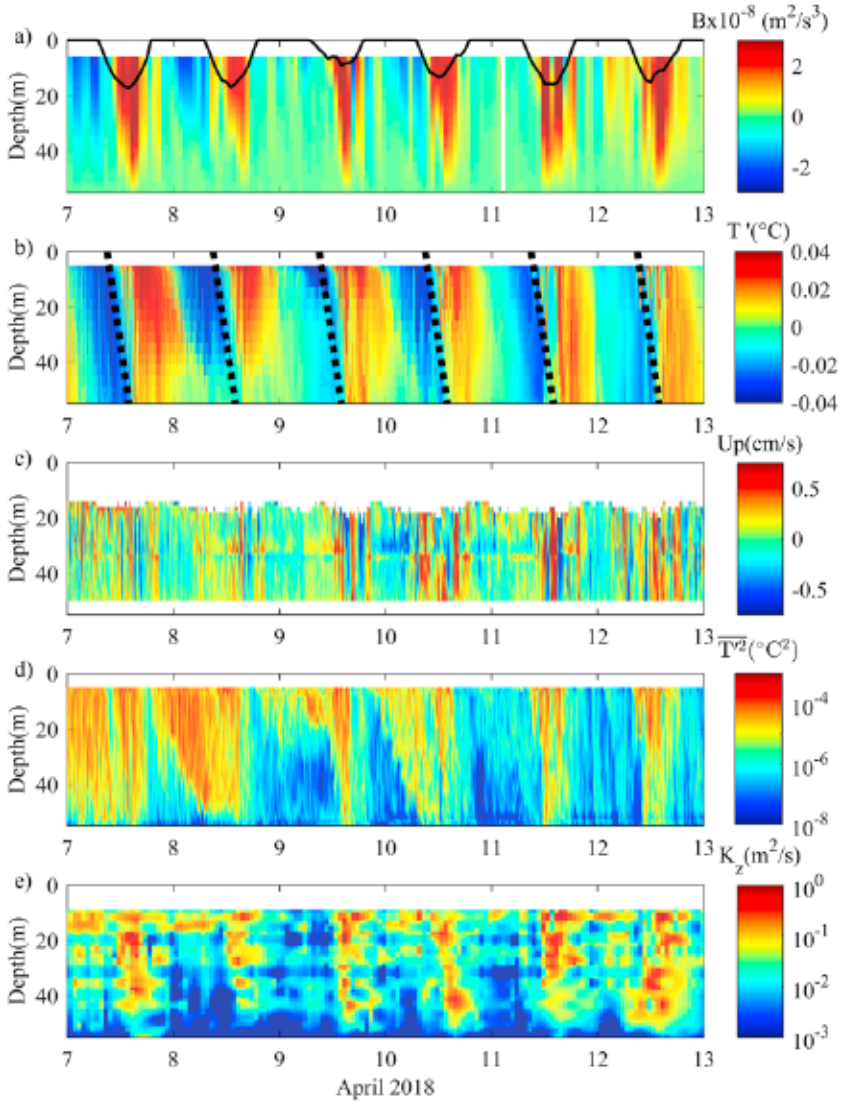

Figure 4. Turbulent mixing parameters observed over the convective period (7–13 April), including (a) buoyancy flux (B) and scaled incoming solar radiation (I_o/50; black line), (b) 24-hr detrended temperature fluctuations and mixed layer deepening rate (dashed lines; $dH_{CML}/dt = 12.8$ m/hr), (c) 60 s averaged vertical velocities, (d) temperature variance ($\overline{T'^2}$), and (e) turbulent scalar diffusivity (K_z).

3. Results

Our observations highlight the diurnal cycle of radiative convection, most evident when the water column is warming under weak wind forcing (e.g., 7–12 April, Figures 2–4). When wind forcing is absent ($\tau_{wind} < 0.15$Pa), water column temperatures exhibit a diurnal cycle of (1) developing unstable stratification during daytime solar heating (warm dense water atop cold water) and (2) restoring stable stratification during nighttime cooling (Figure 3). This cycle is seen at all depths (0–55 m), implying full water column connectivity (day and night) and suggesting that average vertical mixing rates are significantly higher than typical observations in stably stratified lakes (Wüest & Lorke, 2003; $K_z = 10^{-6} - 10^{-2}$m^2/s). This elevated mixing occurs in spite of weak currents and vertical shear (median speed: 6.3 cm/s; Figure 2b), suggesting that it is convection, not shear, that drives mixing during periods of weak wind forcing.

Daily patterns in vertical temperature profiles during convective periods demonstrate the importance of both radiative convection and surface cooling on diurnal stratification dynamics (Figure 3). After sunrise (~08:00), penetrative solar radiation quickly warms surface waters, creating unstable stratification. These warming surface temperatures increase the density of water over the time-varying photic zone, creating

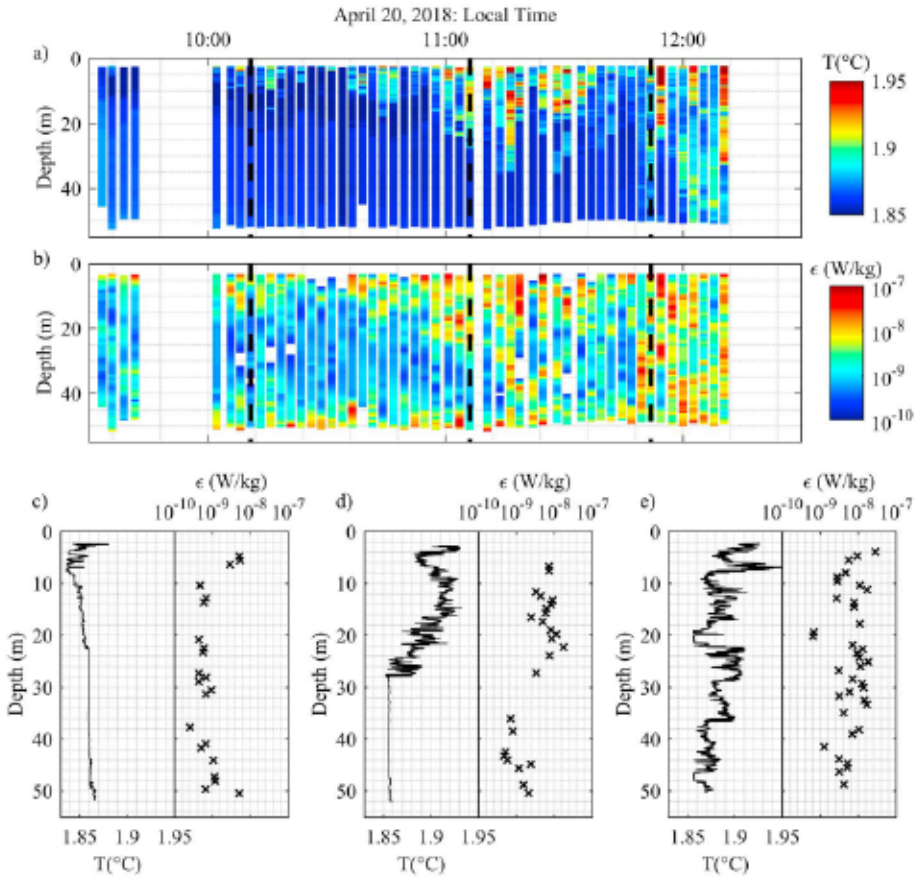

Figure 5. Representative microstructure measurements of (a) temperature and (b) turbulent kinetic energy dissipation (ε) observed on 20 April. Includes (c–e) individual profiles of temperature and dissipation, with measurement times indicated by vertical lines in (a and b).

weakly unstable density stratification ($N^2 = -10^{-5}$ rad^2/s^2) and forcing convective mixing as the denser surface waters sink toward the lakebed. Convective mixing leads to time-lagged increases in water temperatures at all depths throughout the day, with phase-lag calculations (Farmer, 1975), suggesting that the mixed layer deepens at a rate of dH_{CML}/dt=12.8 m/hr from shortly after sunrise (10:00) through ~14:00 local time (Figure 4b), at which point the whole water column warms synchronously until sunset (~18:00). After sunset (Figure 3b), surface temperatures slowly decrease as heat is lost to the atmosphere. Negative nighttime surface heat fluxes restratify the entire water column (55 m), with the depth of stable stratification increasing throughout the night. This cycle repeats at sunrise, with consecutive days of convective mixing increasing full water column temperatures toward the temperature of maximum density.

High-frequency fluctuations at all depths show linkages between turbulence and the broader diurnal cycle of daytime radiative convection and nighttime restratification. Locally calculated Brunt-Väisälä frequencies (N^2, Figure 2e) show strong diurnal variability at all depths during the convective period, with erratic unstable (-10^{-5}rad^2/s^2) density stratification during the day and weakly stable ($+10^{-6}$rad^2/s^2) stratification at night (Figure 2e). Thermal variance $\left(\overline{T'^2}\right)$ is strongly regulated by the convective cycle as well (Figure 4d), showing the steady descent of the actively convective layer during the day and highlighting the disparity between energetic daytime mixing and calmer overnight conditions ($\overline{T'^2}$~10^{-8} versus 10^{-4} °C^2, respectively). The hallmark of convection—vertical motion—is seen in the vertical component of velocity, with magnitudes as high as ±6 mm/s observed throughout the water column (Figure 4c). These velocities, indicative of thermal plumes, agree well with measurements in both ice-covered (Bouffard et al., 2016; Farmer, 1975) and surface-cooled (Jonas, Stips, et al., 2003) lakes, though the mixed layer depth in the current study (max: 55 m) is significantly larger than typical observations (discussed below).

Turbulent kinetic energy dissipation (ϵ) estimates are elevated during convective periods, with vertical structures that match the steady deepening of the mixed layer during daytime warming (Figure 5; no available nighttime profiles). As radiative heating increases water column temperatures throughout the day, patches of warm water grow progressively larger near the surface (Figure 5a). These warmer, unstable waters correspond with dramatically increased turbulence, with dissipation rates almost 2 orders of magnitude larger in unstable versus nominally stable regions (10^{-10} versus 10^{-8} W/kg, respectively). Enhanced dissipation values follow the deepening convective mixed layer throughout the day, with full water column enhancement observed by early afternoon. This 2-order enhancement agrees well with other convective measurements in lakes (ice-covered: Bouffard et al., 2016; surface-cooled: Jonas, Stips, et al., 2003), where measured dissipation rates have been observed to increase from 10^{-10} to 10^{-8} W/kg within the convective mixed layer. Some turbulence enhancement is seen near the bed in the current study, where fewer temperature inversions were observed; this is most likely associated with the compact bottom boundary layer turbulence as described in Cannon and Troy (2018).

The rapid mixed layer growth associated with both daytime convection and overnight restratification (Figure 3) suggests high turbulent mixing rates, and estimates support this inference. Daytime turbulent diffusivity (K_z) estimates during convective periods regularly exceed 10^{-1} m^2/s, with a commensurate mixing timescale of $T_{\text{mix}} \sim \frac{H^2}{K_z} \sim 8.4$ hr. While overnight diffusivities are significantly lower than convective values, the nearly isothermal nature of the water column allows mixing to remain relatively high, with observed diffusivities between 10^{-3} and 10^{-2} m^2/s. For the convective period 7–13 April, average daytime diffusivities at 20-m depth were $8.5 \pm 5.1 \times 10^{-2}$ m^2/s, with nighttime averages of $9.8 \pm 2.1 \times 10^{-3}$ m^2/s (overall average: 1.7×10^{-2} m^2/s).

4. Discussion and Conclusions

This research highlights the importance of radiative convection in setting turbulent mixing characteristics during the spring heating period in large, ice-free lakes. While average hypolimnetic mixing rates measured over the experiment ($K_z = 1.7 \times 10^{-2}$ m^2/s; 7–13 April) agree well with vernal turnover modeling in other large lakes (e.g., Lake Baikal: 5×10^{-2} m^2/s; Schmid et al., 2007), they are significantly elevated relative to stratified conditions, which are more widely reported in physical limnology. In the Laurentian Great Lakes, the waters are typically stratified from May to December (Choi et al., 2012), with measurements suggesting that the vertical diffusivity (K_z) ranges from 10^{-7} to 10^{-4} m^2/s in shallow (<30 m) waters (Hamidi et al., 2015; Rao et al., 2008). Our own (ongoing) research at this measurement location suggests that stratified mixing rates rarely exceed 10^{-3} m^2/s, with full water column averages below 10^{-5} m^2/s. This mixing enhancement is especially important for dispersing bottom-sourced nutrients into the water column. Seasonal measurements of soluble reactive phosphorus show dramatic increases in both magnitude (depth average: +50%) and near-bed (<2 mab) vertical flux (~150x) during the well-mixed period, with repeated convective mixing allowing nutrients to stay in suspension at high concentrations. These differences between the stratified summer and convective spring highlight the importance of seasonality in temperate lakes, where differences in vertical transport have dramatic consequences for biological and chemical cycles.

Recent work on radiative convection in higher-latitude lakes has shown the importance of this mechanism in driving *under-ice* mixing and vertical transport (Bouffard & Wüest, 2019). The *ice-free* radiative convection that we describe here for Lake Michigan follows a similar diurnal pattern of turbulent enhancement in the photic zone, steady deepening of the mixed layer during daytime heating, and restratification during the night (Bouffard et al., 2019). However, the vertical extent and rate of convective mixed-layer deepening that we describe in Lake Michigan (full 55-m depth; $dH_{CML}/dt \sim 12.8$ m/hr; $w \approx 6$ mm/s) appears to be larger and more vigorous than the under-ice analog, for which radiative convection has been shown to influence only the uppermost 5–30 m of the water column (Bouffard et al., 2016; Bouffard et al., 2019; Forrest et al., 2008; Mironov et al., 2002). This was also reported by Austin (2019), who showed that ice-free radiative convection drove enhanced vertical velocities (~1 cm/s) and mixed layer depths (180 m) in Lake Superior during the spring heating period. Below, we discuss several likely reasons for this enhancement and try to generalize our results to other large, midlatitude lakes.

With respect to ice-free radiative convection, Lake Michigan and Lake Huron, to which it is connected, uniquely benefit from several factors that make the mechanism potentially more important here than in other large lakes. Perhaps most obviously, Lake Michigan experiences a much larger amount of downwelling solar irradiance than the ice-covered lakes for which radiative convection has been documented. This is due both to the lack of an albedo effect of the ice, which permits only a small fraction (<50%; Bouffard et al., 2019) of the radiation to reach the water, and the lower latitude of the lake itself. Ice-covered lakes that have been studied are generally at higher latitudes and therefore receive both lower magnitudes and durations of solar irradiance during the day than a relatively low latitude temperate lake like Lake Michigan. While Lake Michigan experiences partial ice cover (Figure 1), the comparatively low latitude (i.e., high winter irradiance) means that ice cover is generally small, and getting smaller with climate change (Wang et al., 2011), negating the ice albedo effect described above. Additionally, the invasion and profundal expansion of quagga mussels in the past two decades has increased water clarity in both lakes to the point where secchi depths now regularly exceed 20 m (Barbiero et al., 2018), allowing sunlight to penetrate and directly heat the water to great depths. Together, these factors dramatically increase the overwinter heat input to the lakes, allowing ice-free radiative convection to play a potentially larger role in winter mixing for Lakes Michigan and Huron than for other large lakes around the world.

The importance of shear in the present observations of convection-dominated mixing should not be overlooked. Fully ice covered lakes have no surface wind shear, which means that there is little water column shear to generate turbulence and no opportunity for waves to directly inject turbulence at the surface. Even for the *purely convective* periods that we highlight in this paper, some wind and water column shear is always present. In fact, while the wind shear observed over the current deployment is on par with the multidecadal average (not shown), spring winds often exceed 15 m/s ($\tau \approx 0.5$ Pa) at this sample site. The mixing paradigm most appropriate for ice-free radiative convection is therefore not *convection- or shear-driven mixing* but rather a combination of the two mechanisms. Even weak shear may provide low levels of turbulence that provide necessary perturbations supporting the continuous generation and maintenance of convectively driven mixing. Spring convection is further complicated by the duality of generation mechanisms; radiative convection dominates mixing during the day (as observed here), but surface fluxes may also drive overnight convection when air temperatures are warmer than surface waters. Our current observations suggest that shear, penetrative solar radiation, and surface heat fluxes are all important for accurately modeling mixing during the vernal turnover. Future work at this sample site will be focused on fully resolving these parameters over the entire turnover period.

Much of the work examining mixing in Lake Michigan, including the present study, is motivated by a desire to understand the interplay between turbulent mixing and the ability of benthic-dwelling invasive quagga mussels to filter the water column. As invasive mussels have filtered the lake, they have effectively increased the apparent settling velocity over the convective spring, driving faster delivery of nutrients and phytoplankton to the lake bed (Chapra & Dolan, 2012; Shen et al., 2018). With vertically averaged diffusivities of 4.9×10^{-2} m^2/s during the day and 1.4×10^{-2} m^2/s overnight, commensurate water column mixing timescales ($T_{\text{mix}} \sim \frac{H^2}{K_z}$) are 17 and 60 hr, respectively. Comparing these mixing timescales to mussel filtration timescales for deep waters (4–10 days; Vanderploeg et al., 2010; Barbiero et al., 2018), our results support the well-mixed assumption used to analyze the interplay between mussel filtration and phytoplankton growth. In essence, this work demonstrates that mussels in deep waters should not suffer a food delivery limitation during the convective spring as they may during the stratified summer period. However, there is much future work needed in order to quantify how spring mixing varies both spatially and temporally, including a careful accounting of the longer-term cycle of radiative convection as water column temperatures progress toward the temperature of maximum density and an analysis of long-term warming trends that may weaken this important mixing mechanism.

Acknowledgments
We thank the captain and crew of the R/V *Neeskay* and *Osprey* for their invaluable support during field work on Lake Michigan. This project was funded by the National Science Foundation, Division of Ocean Sciences (OCE-1658156 and OCE-1658390). The data used in this publication are available from the Biological and Chemical Oceanography Data Management Office (Troy et al., 2019a; Troy et al., 2019b; Troy et al., 2019c).

References

Austin, J. A. (2019). Observations of radiatively driven convection in a deep lake. *Limnology and Oceanography*. https://doi.org/10.1002/lno.11175

Barbiero, R. P., Lesht, B. M., Warren, G. J., Rudstam, L. G., Watkins, J. M., Reavie, E. D., et al. (2018). A comparative examination of recent changes in nutrients and lower food web structure in Lake Michigan and Lake Huron. *Journal of Great Lakes Research*, *44*, 573–589. https://doi.org/10.1016/j.jglr.2018.05.012

Beletsky, D., & Schwab, D. J. (2001). Modeling circulation and thermal structure in Lake Michigan: Annual cycle and interannual variability. *Journal of Geophysical Research, 106*(C9), 19,745–19,771. https://doi.org/10.1029/2000JC000691

Bennett, E. B. (1978). Characteristics of the thermal regime of Lake Superior. *Journal of Great Lakes Research, 4*(3–4), 310–319. https://doi.org/10.1016/S0380-1330(78)72200-8

Bluteau, C. E., Jones, N. L., & Ivey, G. N. (2016). Estimating turbulent dissipation from microstructure shear measurements using maximum likelihood spectral fitting over the inertial and viscous subranges. *Journal of Atmospheric and Oceanic Technology, 33*(4), 713–722. https://doi.org/10.1175/JTECH-D-15-0218.1

Bouffard, D., & Wüest, A. (2019). Convection in lakes. *Annual Review of Fluid Mechanics, 51*(1), 189–215. https://doi.org/10.1146/annurev-fluid-010518-040506

Bouffard, D., Zdorovennov, R. E., Zdorovennova, G. E., Pasche, N., Wüest, A., & Terzhevik, A. Y. (2016). Ice-covered Lake Onega: Effects of radiation on convection and internal waves. *Hydrobiologia, 780*(1), 21–36. https://doi.org/10.1007/s10750-016-2915-3

Bouffard, D., Zdorovennova, G., Bogdanov, S., Efremova, T., Lavanchy, S., Palshin, N., et al. (2019). Under-ice convection dynamics in a boreal lake. *Inland Waters*, 1–20. https://doi.org/10.1080/20442041.2018.1533356

Boyce, F. M., Donelan, M. A., Hamblin, P. F., Murthy, C. R., & Simons, T. J. (1989). Thermal structure and circulation in the great lakes. *Atmosphere-Ocean, 27*(4), 607–642. https://doi.org/10.1080/07055900.1989.9649358

Cannon, D. J., & Troy, C. D. (2018). Observations of turbulence and mean flow in the low-energy hypolimnetic boundary layer of a large lake. *Limnology and Oceanography, 63*(6), 2762–2776. https://doi.org/10.1002/lno.11007

Chapra, S. C., & Dolan, D. M. (2012). Great Lakes total phosphorus revisited: 2. Mass balance modeling. *Journal of Great Lakes Research, 38*(4), 741–754. https://doi.org/10.1016/j.jglr.2012.10.002

Choi, J., Troy, C. D., Hsieh, T.-C., Hawley, N., & McCormick, M. J. (2012). A year of internal Poincaré waves in southern Lake Michigan. *Journal of Geophysical Research, 117*, C07014. https://doi.org/10.1029/2012JC007984

Church, P. E. (1947). Convection in the annual temperature cycle of Lake Michigan. *Annals of the New York Academy of Sciences, 48*(8), 789–799. https://doi.org/10.1111/j.1749-6632.1947.tb38491.x

Farmer, D. M. (1975). Penetrative convection in the absence of mean shear. *Quarterly Journal of the Royal Meteorological Society, 101*(430), 869–891. https://doi.org/10.1002/qj.49710143011

Forrest, A. L., Laval, B. E., Pieters, R., & Lim, D. S. S. (2008). Convectively driven transport in temperate lakes. *Limnology and Oceanography, 53*(5), 2321–2332. https://doi.org/10.4319/lo.2008.53.5_part_2.2321

Gill, A. (1982). *Atmosphere-Ocean Dynamics*, (Vol. 662). New York: Academic Press.

Goodman, L., Levine, E. R., & Lueck, R. G. (2006). On measuring the terms of the turbulent kinetic energy budget from an AUV. *Journal of Atmospheric and Oceanic Technology, 23*(7), 977–990. https://doi.org/10.1175/JTECH1889.1

Hamidi, S. A., Bravo, H. R., Val Klump, J., & Waples, J. T. (2015). The role of circulation and heat fluxes in the formation of stratification leading to hypoxia in Green Bay, Lake Michigan. *Journal of Great Lakes Research, 41*(4), 1024–1036. https://doi.org/10.1016/J.JGLR.2015.08.007

Hampton, S. E., Galloway, A. W. E., Powers, S. M., Ozersky, T., Woo, K. H., Batt, R. D., et al. (2017). Ecology under lake ice. *Ecology Letters, 20*(1), 98–111. https://doi.org/10.1111/ele.12699

Jonas, T., Stips, A., Eugster, W., & Wüest, A. (2003). Observations of a quasi shear-free lacustrine convective boundary layer: Stratification and its implications on turbulence. *Journal of Geophysical Research, 108*(C10), 3328. https://doi.org/10.1029/2002JC001440

Jonas, T., Terzhevik, A. Y., Mironov, D. V., & Wüest, A. (2003). Radiatively driven convection in an ice-covered lake investigated by using temperature microstructure technique. *Journal of Geophysical Research, 108*(C6), 3183. https://doi.org/10.1029/2002JC001316

Leshkevich, G., Chu, P., & Liu, S. (2018). NOAA Great Lakes CoastWatch. Retrieved June 1, 2019, from https://coastwatch.glerl.noaa.gov/

Lueck, R. (2013). Calculating the rate of dissipation of turbulent kinetic energy, 22. Retrieved from http://files/47/Lueck - Calculating the Rate of Dissipation of Turbulent K.pdf

Macoun, P., & Lueck, R. (2004). Modeling the spatial response of the Airfoil Shear Probe using different sized probes. *Journal of Atmospheric and Oceanic Technology, 21*(2), 284–297. https://doi.org/10.1175/1520-0426(2004)021<0284:MTSROT>2.0.CO;2

Martin, J. L., McCutcheon, S. C., & Schottman, R. W. (1999). *Hydrodynamics and Transport for Water Quality Modeling*. Boca Raton: Lewis Publishers.

Mironov, D., Terzhevik, A., Kirillin, G., Jonas, T., Malm, J., & Farmer, D. (2002). Radiatively driven convection in ice-covered lakes: Observations, scaling, and a mixed layer model. *Journal of Geophysical Research, 107*(C4), 3032. https://doi.org/10.1029/2001JC000892

Mosley, C., & Bootsma, H. (2015). Phosphorus recycling by profunda quagga mussels (Dreissena rostriformis bugensis) in Lake Michigan. *Journal of Great Lakes Research, 41*, 38–48. https://doi.org/10.1016/J.JGLR.2015.07.007

Osborn, T. R. (1974). Vertical profiling of velocity microstructure. *Journal of Physical Oceanography, 4*(1), 109–115. https://doi.org/10.1175/1520-0485(1974)004<0109:VPOVM>2.0.CO;2

Rao, Y. R., Hawley, N., Charlton, M. N., & Schertzer, W. M. (2008). Physical processes and hypoxia in the central basin of Lake Erie. *Limnology and Oceanography, 53*(5), 2007–2020. https://doi.org/10.4319/lo.2008.53.5.2007

Ruddick, B., Anis, A., & Thompson, K. (2000). Maximum likelihood spectral fitting: The Batchelor Spectrum. *Journal of Atmospheric and Oceanic Technology, 17*(11), 1541–1555. https://doi.org/10.1175/1520-0426(2000)017<1541:MLSFTB>2.0.CO;2

Scavia, D., & Bennett, J. R. (1980). Spring transition period in Lake Ontario—A numerical study of the causes of the large biological and chemical gradients. *Canadian Journal of Fisheries and Aquatic Sciences, 37*(5), 823–833. https://doi.org/10.1139/f80-111

Schmid, M., Batist, M. D., Granin, N. G., Kapitanov, V. A., McGinnis, D. F., Mizandrontsev, I. B., et al. (2007). Sources and sinks of methane in Lake Baikal: A synthesis of measurements and modeling. *Limnology and Oceanography, 52*(5), 1824–1837. https://doi.org/10.4319/lo.2007.52.5.1824

Shen, C., Liao, Q., Bootsma, H. A., Troy, C. D., & Cannon, D. (2018). Regulation of plankton and nutrient dynamics by profundal quagga mussels in Lake Michigan: A one-dimensional model. *Hydrobiologia, 815*(1), 47–63. https://doi.org/10.1007/s10750-018-3547-6

Sommer, U., Adrian, R., de Senerpont Domis, L., Elser, J. J., Gaedke, U., Ibelings, B., et al. (2012). Beyond the Plankton Ecology Group (PEG) model: Mechanisms driving plankton succession. *Annual Review of Ecology, Evolution, and Systematics, 43*(1), 429–448. https://doi.org/10.1146/annurev-ecolsys-110411-160251

Tanaka, M., Girard, G., Davis, R., Peuto, A., & Bignell, N. (2001). Recommended table for the density of water between 0 °C and 40 °C based on recent experimental reports. *Metrologia, 38*(4), 301–309. https://doi.org/10.1088/0026-1394/38/4/3

Troy, C., Bootsma, H., Cannon, D., & Liao, Q. (2019b). Microstructure profiles at Station AT55 in Lake Michigan aboard the R/V Osprey from 2018-04-05 to 2018-04-20. Biological and Chemical Oceanography Data Management Office (BCO-DMO). Dataset version 2019-05-15. https://doi.org/10.1575/1912a/bco-dmo.768011.1.

Troy, C., Bootsma, H., Cannon, D., & Liao, Q. (2019c). Velocity observations from a mooring at Station AT55 in Lake Michigan from 2018-04-05 to 2018-04-20. Biological and Chemical Oceanography Data Management Office (BCO-DMO). Dataset version 2019-05-14. https://doi.org/10.1575/1912b/bco-dmo.767737.1

Troy, C., Bootsma, H., Cannon, D., & Liao, Q. (2019a). Temperature mooring data collected at Station AT55 in Lake Michigan from August 1, 2017 to April 20, 2018. Biological and Chemical Oceanography Data Management Office (BCO-DMO). Dataset version 2019-05-16. https://doi.org/10.1575/1912/bco-dmo.734541.2

Troy, C., Cannon, D., Liao, Q., & Bootsma, H. (2016). Logarithmic velocity structure in the deep hypolimnetic waters of Lake Michigan. *Journal of Geophysical Research: Oceans, 121*, 949–965. https://doi.org/10.1002/2014JC010506

Vanderploeg, H. A., Liebig, J. R., Nalepa, T. F., Fahnenstiel, G. L., & Pothoven, S. A. (2010). Dreissena and the disappearance of the spring phytoplankton bloom in Lake Michigan. *Journal of Great Lakes Research, 36*, 50–59. https://doi.org/10.1016/j.jglr.2010.04.005

Wang, J., Bai, X., Hu, H., Clites, A., Colton, M., & Lofgren, B. (2011). Temporal and spatial variability of Great Lakes ice cover, 1973-2010*. *Journal of Climate, 25*(4), 1318–1329. https://doi.org/10.1175/2011JCLI4066.1

Wüest, A., & Lorke, A. (2003). Small-scale hydrodynamics in lakes. *Annual Review of Fluid Mechanics, 35*(1), 373–412. https://doi.org/10.1146/annurev.fluid.35.101101.161220

Yang, B., Young, J., Brown, L., & Wells, M. (2017). High-frequency observations of temperature and dissolved oxygen reveal under-ice convection in a large lake. *Geophysical Research Letters, 44*, 12,218–12,226. https://doi.org/10.1002/2017GL075373